Repetitively enhanced neural networks method for complex engineering design optimisation problems

N. Van Nguyen
nhuvan@gmail.com
J-W. Lee
jwlee@konkuk.ac.kr
M. Tyan and S. Kim
Aerospace Information Engineering
Konkuk University
Seoul
South Korea

ABSTRACT

A Repetitively Enhanced Neural Networks (RENN) method is developed and presented for complex and implicit engineering design problems. The enhanced neural networks module constructs an accurate surrogate model and avoids over-fitting during neural networks training from supervised learning data. The optimiser is executed by the enhanced neural networks models to seek a tentative optimum point. It is repetitively added into the supervised learning data set to refine the surfaces until the RENN tolerance is reached. The RENN method demonstrates the effectiveness and feasibility for a 2D highly non-linear numerical example and the structure design of a two-member frame reaching a convergent solution at 10 and 15 iterations at the maximum error of 1% when compared with the exact solution. Then, the RENN method is applied for a long endurance unmanned aerial vehicle (UAV) aerofoil design optimisation. A Class/Shape function transformation (CST) geometry parameterisation method represents an accurate UAV aerofoil with ten geometry design variables. The high-fidelity analysis solver with structured mesh is used for

Paper No. 4243. Manuscript received 25 July 2014, revised version received 19 April 2015, accepted 8 May 2015.

https://doi.org/10.1017/S0001924000011234 Published online by Cambridge University Press

a UAV aerofoil design problem. Using the RENN method, an optimal UAV aerofoil is obtained using 88 high fidelity evaluations at an error of 1·24%. The process reduces the computational time by 81·2% compared with the full high fidelity model. The optimal aerofoil shows a drag reduction of 10·8% in the cruise condition and an improvement in the maximum lift coefficient and stall angle-of-attack when compared with the baseline AG24 aerofoil.

NOMENCLATURE

α_{stall}	stall angle-of-attack, in degrees
b	network bias
C_d	2D aerofoil drag coefficient
C_l	2D aerofoil lift coefficient
C_{lmax}	maximum lift coefficient
E_D	sum of squared errors
E_W	sum of squares of the network weights
L/D	lift over drag ratio
t/c	aerofoil thickness ratio
X	training input
Z	target output
Y	outputs from network
W	network weight
BPNN	Back-Propagation Neural Networks
CST	Class/Shape Function Transformation
DOE	Design Of Experiment
ENN	Enhanced Neural Networks
FFD	Full Factorial Design
NN	Neural Networks
RSM	Response Surface Methodology
RENN	Repetitively Enhanced Neural networks
UAV	Unmanned Aerial Vehicle

1.0 INTRODUCTION

In complex engineering design problems, the output signals normally appear in implicit and highly nonlinear forms with input signals. Shen *et al* combined artificial networks and genetic algorithms to determine an optimal plastics injection molding process, in which the quality index of the volumetric shrinkage variation in the part is the complex non-linear relationship between the process conditions, such as injection packing, cooling ejections, and quality control applications[1]. Plastics injection molding problems were also researched and optimised by B. Ozcelik *et al*[2] and S.L. Mok[3]. The implicit and complex cost functions are warpage, sink marks, and initial process parameters for injection molding problems[2,3]. Multidisciplinary aerospace vehicle system design optimisation has many difficulties to use high-fidelity solvers, such as computational fluid dynamics (CFD) for aerodynamics modules and the finite element methods (FEM) solver for the structure module directly to design optimisation. Kyung *et al* introduced the reduced-order model using artificial neural networks for an aero-structural design optimisation[4]. The proposed algorithm has the capability to efficiently and accurately predict the aerodynamics and structure performance of

https://doi.org/10.1017/S0001924000011234 Published online by Cambridge University Press

the wing. The minimisation of wing weight demonstrates more efficient design than a conventional design method using a second-order response model[4]. Additionally, artificial neural networks (ANN) is also implemented efficiently to interpolate the aerodynamics pressure loads from the CFD analysis to finite element methods for one way unmanned aerial vehicle (UAV) fluid structure interaction (FSI)[5]. The results show good agreement with the actual pressure profile on the aircraft using ANN compared with 2D curve fitting with higher order polynomials[5]. Moreover, ANN was used for an inverse aerofoil design problem by K. Athar *et al* The feed-forward back propagation, generalised regression, and radius basic neural networks were implemented to perform an inverse aerofoil design for a given C_p-distribution[6]. Neural networks was also used to investigate the flush air data sensing system for small unmanned air vehicles at speeds as low as Mach 0·07 due to its good generalisation capabilities and compact structure[7]. M. R. Man *et al* applied ANN to redesign the turbine aerofoil from a modern jet engine[8]. K. K. Saijal indicated that the flap power and vibration minimisation of helicopter rotors are highly non-linear, and polynomials are not able to fit these objective functions. Therefore, neural networks was implemented to approximate both the flap power and the helicopter vibration for a multi-objective function[9]. The two metal models demonstrated a 27% reduction in hub vibration and a 45% reduction in flap power[9]. In addition, ANN was also applied for subsonic aircraft design optimisation at the conceptual design stage due to its accurate regression and parallel computing[10]. S. Wei *et al* used neural networks for global aerodynamics and rocket propulsion components to avoid the computational loads during the optimisation loop. The method helps improve the design of practical devices, such as wing aerodynamics, turbulent diffuser flows , gas-gas injectors, and supersonic turbines[11]. A. Mehran *et al* applied ANN efficiently for the decision making process in the early aircraft design stage. The results demonstrated the effectiveness of the ANN approach in the preliminary aircraft design process. The error between the ANN models and the actual value was less than 10% for the take-off wing loading and the take-off thrust loading[12]. S. Manoranjan *et al* presented a method using neural networks to estimate the separation point and stall speed of cascaded fins. The results indicated that an increase in the number of fins in the cascade increases the stall angle and lift curve slope[13]. F.H. Joseph *et al* also presented a direct trajectory optimisation method using neural networks approximation methods to reduce the computational requirements and to provide fast computation of the gradient when compared with direct and pseudo-spectral collocation methods[14]. The ejection velocity of an escapee system was also predicted using back-propagation neural networks with the sequencer control subsystem and the parachute shooting time. H. Abdurrahman introduced a method for aerofoil design by combining an evolutionary algorithm and neural networks to greatly improve the exploration power of the algorithm and reduce the computational load during the genetic algorithm while maintaining the robustness of the solution[15]. In addition, N.V. Queipo *et al* introduced the comprehensive discussion about surrogate based models including Radius Basic Function (RBF) for analysis and design optimisation. The case study of multi-objective liquid-rocket injector design to highlight the surrogate based model state of art[16]. A.I.J. Forrester *et al* reviewed the recent advances in surrogate-based optimisation including RBF, Kriging, and support vector regression. The strengths and weaknesses of each method are presented to bring the efficient global optimisation closer to reality[17]. Moreover, S. Koziel *et al* mentioned that simulation-based objective functions are often discontinuous, non-differentiable, and inherently noisy. Another, the computation load in objective analysis is extremely high. Hence, feasible resolving of these functions can be accomplished using surrogate models[18]. S. Koziel *et al* proposed several surrogate based models for aerospace applications including a multi-level surrogate-based aerofoil shape optimisation[19], a variable-resolution models and space mapping for transonic aerofoil aerodynamic shape optimisation[20,21].

https://doi.org/10.1017/S0001924000011234 Published online by Cambridge University Press

Therefore, neural networks is a promising surrogate model due to its accurate generalisation and parallel computation capabilities in complex engineering design problems, especially in aerospace vehicle design optimisation applications. A repetitively enhance neural networks (RENN) method is proposed in this study. RENN is composed of an enhanced neural network that improves upon the conventional neural networks and avoids over-fitting. The initialisation of weight and biases for neural network are investigated to select the effective starting points for training network efficiently and accelerating the convergence. In addition, a Back-propagation algorithm and Bayesian learning are used to prevent over-fitting of network. The optimal point is repetitively added to refine the neural networks surface efficiently after the optimisation loop terminates. The RENN demonstrates the effectiveness and feasibility with a 2D high non-linear numerical example and two-member structure frame design with three design variables and implicit constraints. Then, a long endurance UAV aerofoil design optimisation is performed by implementing the RENN method with ten aerofoil geometry design variables and high-fidelity analysis solvers.

2.0 REPETITIVELY ENHANCED NEURAL NETWORKS (RENN) PROCESS

The overall process of RENN is presented in Fig. 1. Engineering design problems start with design formulation, in which the objective, constraints functions, design variables and space are defined. The experimental points are selected using Design of Experiment (DoE) methods, such as

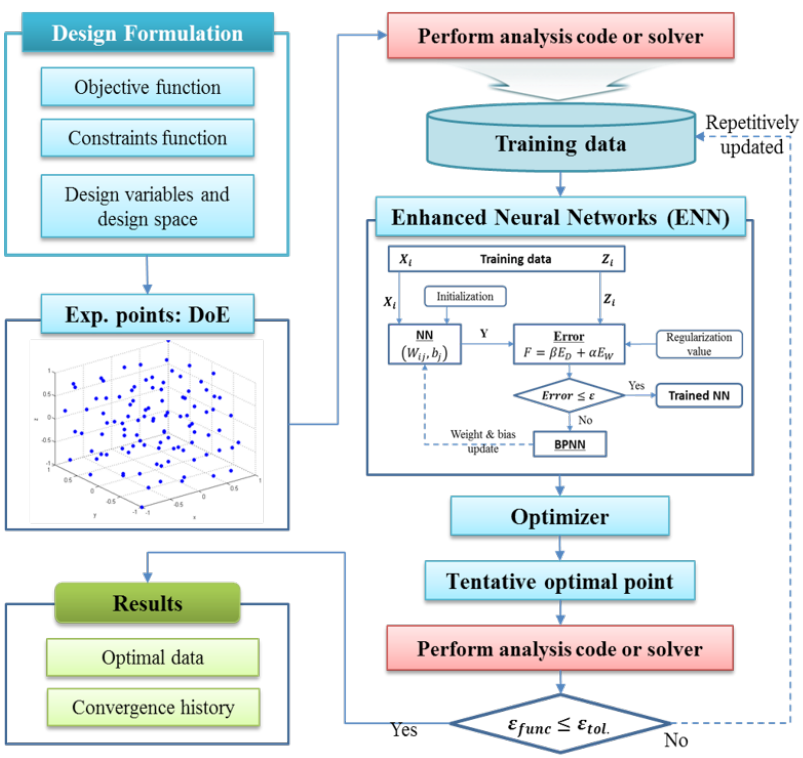


Figure 1. Repetitively Enhanced Neural Network (RENN).

https://doi.org/10.1017/S0001924000011234 Published online by Cambridge University Press

D-optimality and Latin Hypercube[22,23]. Then, the set of experimental points is sent to an analysis code or solver to obtain the responses, including the objective and constraints values. Training or supervised learning data are obtained to construct the surrogate models by implementing enhanced neural networks (ENN), as shown in Fig. 1. The hybrid optimiser is executed to search for the first tentative optimal point The analysis code or solver is performed on the tentative optimal point to check the difference between the surrogate model ENN and the analysis code. If the difference does not satisfy the tolerance, it is added into the training data to refine the ENN models; if it does satisfy the tolerance, the results are obtained, as shown in Fig. 1.

2.1 Multilayer neural networks structure

A Neural Network (NN) is a computational structure, consisting of highly interconnected processing units called neurons[24]. The multilayered neural network architecture is normally composed of three layers, which are inputs, hidden, and outputs layers, as shown in Fig. 2. This neural networks structure is able to complete the approximation tasks of any nonlinear function[24].

The X_i inputs layers receive the input data from a training data set, and then it is multiplied by the weight $W_{i,j}$ and added to the bias to provide for the j hidden layers, as shown in Fig. 2. The transfer function in the hidden layer is used to estimate the output Y_j of the neuron. The mathematical neural networks formulation is written as Equations (1) and (2).

$$a_j = \sum W_{i,j} X_i + b_j \quad \ldots (1)$$

$$Y_j = f(a_j) = f(\sum W_{ij} X_i + b_j) \quad \ldots (2)$$

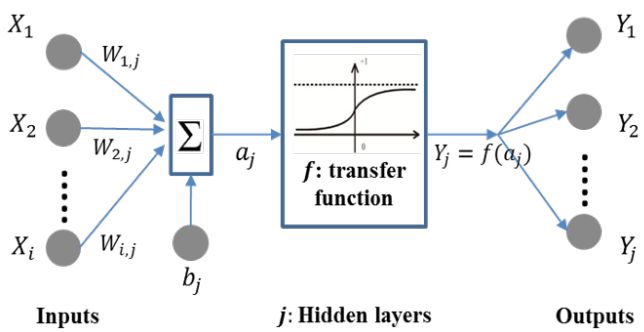


Figure 2. Multilayer neural networks structures.

2.2 Weights and biases initialisation

The initial weight and bias affect the convergence of neural networks. Hence, Nguyen-Widrow proposed a method to initialise the weights and biases effectively during the NN training process[25]. The initial weights are selected as $W_i = 0{\cdot}7H_i^{(25)}$ to accelerate the convergence of neural network, where H_i are the hidden nodes; then the bias initialisations b_j are uniform random numbers between $-W_i$ and W_i.

2.3 Transfer function

The transfer function is used to convert the weighted inputs and biases into outputs layers. The hard limit, linear, tanh-sigmoid and log-sigmoid transfer functions are most commonly used, as listed in Table 1[24].

https://doi.org/10.1017/S0001924000011234 Published online by Cambridge University Press

Table 1
Common transfer function in neural networks

Transfer function	Equation	Range
Hard limit	$f(x) = \{0, \text{if } x < 0 \text{ or } 1 \text{ if } x\}$	(0,1)
Linear	$f(x)$	
Tanh-sigmoid	$f(x) = (e^{x} - e^{-x})\ (e^{x} + e^{-x})$	(–1,1)
Log-sigmoid	$f(x)$	(0,1)

2.4 Enhanced back-propagation neural network

The enhanced neural networks (ENN) start with the training data set or supervised learning methods. The initialisation of weights and bias are based on the Nguyen-Widrow method[25] to accelerate the convergence of networks, as shown in Fig. 3.

The Bayesian learning approach, which is integrated into a back propagation neural network (BPNN)[26], is used to prevent over-fitting and improve the generalisation, as shown in Fig. 3. Typically, the training aims to reduce the modified error function, which is composed of the sum of squared errors and network weights, as shown in Equation (3);

$$F = \beta E_D + \alpha E_W \quad \ldots (3)$$

where $E_D = \sum_j \tfrac{1}{2} (Z_j - Y_j)^2$ the sum of squared errors

$E_W = \sum_{ij} \tfrac{1}{2} W_{if}^2$ the sum of squares of the network weights

The regularisation value is set by considering the effect of the network weights and bias error in the modified error function, as shown in Equation (3), to avoid over-fitting in the trained networks. If the error is not satisfied, the back-propagation algorithm is used to revise the weight and bias in the neural network models, as shown in Fig. 3. After the error satisfies the tolerance, the trained networks are obtained to provide the optimiser module.

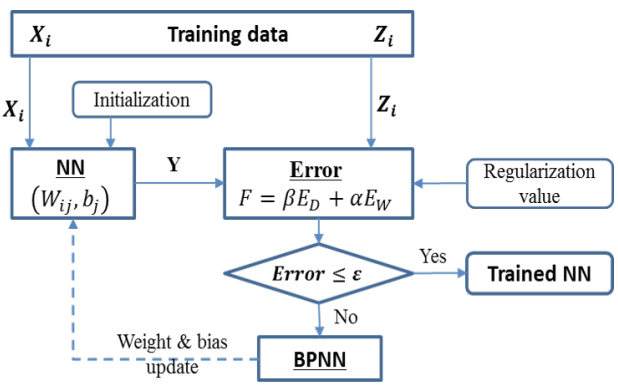


Figure 3. Enhanced Neural Networks (ENN) and Bayesian learning integration.

2.5 Convergence criteria

The convergence criteria are set to terminate the network training process. To avoid over-fitting of the training data, the regularisation value is set. In addition, the training data are divided into the training data and validation data[27].

https://doi.org/10.1017/S0001924000011234 Published online by Cambridge University Press

2.6 optimiser

Sequential Quadratic Programming (SQP), which is a gradient-based method (GBM), is used as an optimiser to search for an optimum point and reduce the computational time during the optimisation loop and repetitive process[27,28].

3.0 THE NUMERICAL DEMONSTRATION OF THE RENN METHOD

3.1 2D numerical example

Minimise;

$$f(x) = -3{\cdot}26 + 3x_1^2 - 2{\cdot}02e^{x_1x_2} + \frac{1}{-0{\cdot}378+0{\cdot}881x_2-0{\cdot}825x_2^2} \quad \ldots (4)$$

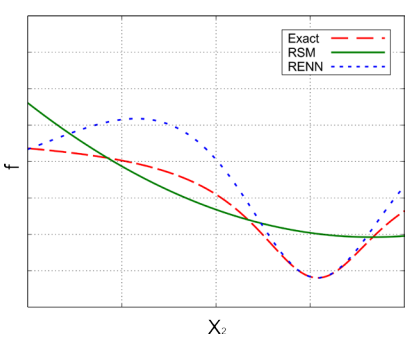
Bounds: $-1 \leq x_1, x_2 \leq 1$

This function was selected due to its high nonlinearity. The function consists of exponential and fractional terms that could be encountered in engineering applications.

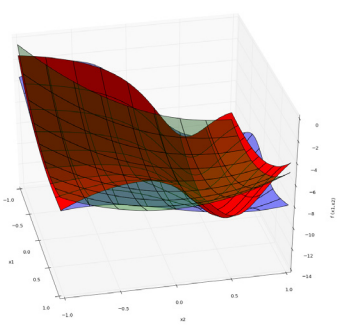
Six design experimental points are selected using the Latin Hypercube method to run the RENN. The convergent results of the 2D numerical example are obtained after ten iterations, as shown in Fig. 5. Hence, sixteen total experimental points are required to obtain the optimum point, as shown in Table 2, with 1·02% error compared with the exact value. The 16 experimental points are generated using the 4 level full factorial designs (FFD)[22,23] to construct a response surface methodology (RSM) model and search for an optimum point, as shown in the Table 2. The error is 18·96% compared with the exact solution when the same experimental points are used with the RENN method.

Table 2
2D numerical example results and comparison

Method	X_1	X_1	f values	Error (%)	Exp. points
Exact Function	–0·203	0·54	–12·39	–	
RSM	–0·62	1·0	–10·04	18·96	16
RENN	–0·175	0·489	–12·264	1·02	16



(a)



(b)

Figure 4. RENN method compared to the exact values and RSM function.

https://doi.org/10.1017/S0001924000011234 Published online by Cambridge University Press

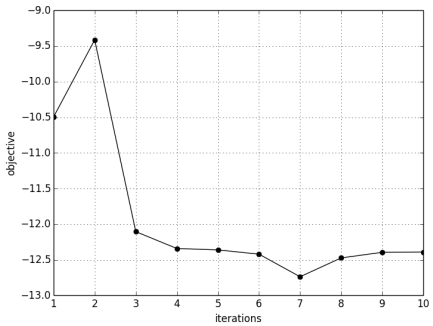


Figure 5. 2D numerical example convergence history for the RENN method.

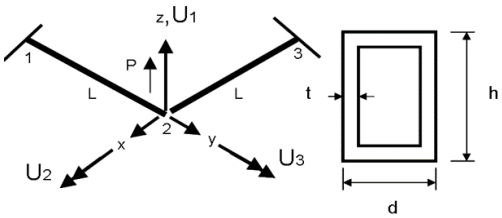


Figure 6. Design of a two-member frame[29].

The exact values, RSM, and RENN curves are also presented in Fig. 4. The RENN method converges into a global optimum point after a few experimental points. In addition, the RENN method globally captures the trend of the exact function in the 3D surface, as shown in Fig. 4. Hence, it is a promising method for complex engineering design optimisation problems.

3.2 Design of a two-member frame

The design of a two-member frame subjected to out-of-plane loads is shown in Fig. 6. Such frames are encountered in numerous automotive, aerospace, mechanical, and structural engineering applications.

The objective function is defined as the minimum of the total volume of the frame, considering two allowable stress constraints, following Von-Misses stress criteria. The three design variables are the width, height and thickness of the frame. The following is the problem statement: Minimise:

$$V(x) = 2L\,(2dt + 2ht - 4h^2) \qquad \ldots (5)$$

Subject to;

$$g_1(x,U) = \frac{1}{\sigma_a^2}(\sigma_1^2 + 3\tau^2) - 1 \le 0 \qquad \ldots (6)$$

$$g_2(x,U) = \frac{1}{\sigma_a^2}(\sigma_2^2 + 3\tau^2) - 1 \le 0 \qquad \ldots (7)$$

$$2{\cdot}5 \le d,h \le 10, 0{\cdot}1 \le t \le 1{\cdot}0\ (in) \qquad \ldots (8)$$

where $\tau = T/2At$, $\sigma_1 = 1/21M_1h$, and $\sigma_2 = 1/21M_2h$ are, respectively, the torsional shear and the bending stresses ineach bar.

The constraints appear in an implicit form with the design variables normally encountered in engineering applications; therefore, to reduce the computational time for large-scale problems, approximation methods are used. The proposed process is applied to this typical design problem, and the results demonstrate the effectiveness and feasibility of the process. In this problem, 23 design points are selected by using the Latin Hypercube method for the first surrogate models construction. A small analysis code is used to obtain theobjective function and constraint responses of the 23 experimental design points.

https://doi.org/10.1017/S0001924000011234 Published online by Cambridge University Press

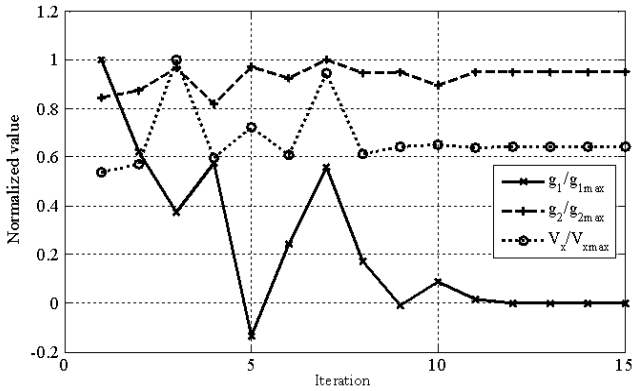


Figure 7. Convergence history constraints and objective functions normalised with respect to the maximum values.

In Table 3, the Repetitive Response Surface Enhancement Technique (RRSET) is an approximation method based on Response Surface Methodology and on the design space transformation[30]. RRSET shows a very accurate result, with an error of 0·525% compared to the exact solution.

The RENN gives an extremely accurate optimum value (0·024%) and design variables; however, the number of experimental points is 38, which is larger than the number used in RRSET and RSM. The two constraints, which are constructed by RENN, indicate active constraints and good agreement with the exact constraint values. From Fig. 7, the constraints and objective functions, which are normalised with respect to the maximum values, converge after 15 iterations.

Table 3
Comparison of repetitively enhanced neural network (RENN)

Method	*d*	*h*	*t*	*V*(*x*)	g_1	g_2	Error (%)	Exp· points
Exact solution	7·798	10	0·1	703·916	7·46E-04	–0·914	–	–
RSM	7·047	7·654	0·1	580·03	–0·012	–0·624	17·6	34
RRSET[24]	7·89	10	0·1	707·62	–	–	0·526	34
RENN	7·82	10	0·1	704·033	1·70E-04	–0·9142	0·024	38

4.0 LONG ENDURANCE UAV AEROFOIL DESIGN

4.1 Design problem definition

UAV aerofoil design is critical to determining the performance characteristics of UAV. A low UAV aerofoil drag at cruise conditions increases the endurance and range performance during operation. A high maximum lift coefficient and stall angle-of-attack decrease the stall speed of a UAV, which allows the UAV to operate at lower speed. Therefore, the UAV aerofoil design optimisation is presented using the high fidelity analysis solver and accurate surrogate models of RENN.

https://doi.org/10.1017/S0001924000011234 Published online by Cambridge University Press

4.2 design methodology

a. Aerofoil geometry parameterisation

Aerofoil geometry is modeled using the class shape function transformations (CST) method[31]. The method makes it possible to represent aerofoil-like shapes using simple analytical functions. The method is becoming increasingly popular for a variety of applications, such as helicopter-blade design[32] or CAD tools for IPPD[33]. The curve is represented as the product of the class and the shape functions. The general form of the mathematical expression is:

$$\zeta(\psi) = C(\psi)S(\psi) \quad \ldots (9)$$

where: $\psi = x/c$ and $\zeta = y/c$

The class function is the function representing the general class of the shapes. For subsonic and transonic aerofoils, the class function is:

$$C(\psi) = \psi^{0\cdot5}\,(1-\psi)^{1\cdot0} \quad \ldots (10)$$

Here, $\psi^{0\cdot5}$ is the term that mathematically provides the round nose shape, and (1-ψ) provides the sharp trailing edge.

The shape function is the function representing the unique shape within a given class. Bernstein polynomials are used as the shape function:

$$S(\psi) = \sum_{i=0}^{n} A_i\, K_i\, \psi^i (1-\psi)^{n-i} \quad \ldots (11)$$

$$K_i = \binom{n}{i} \frac{n!}{i!(n-i)!} \quad \ldots (12)$$

The specific shape of the aerofoil can be obtained by varying the Ai coefficients. A Bernstein polynomial order (BPO) of four makes it possible to fit the existing aerofoil shapes with an accuracy order of 10^{-3}), as seen in Fig. 8. The total number of design variables for an AG24 aerofoil is ten (five for the upper and lower curves).

b. Analysis solver selection

ANSYS fluent® with $k-\varepsilon$ realisable and Spalart-allmaras turbulence models[34] and Xfoil[35] and javafoil[36] panel method tools are compared with the experimental data for an AG24 aerofoil with $Re = 0{\cdot}3 \times 10^6$ [37]. An O-type computational grid with 149 × 75 points and $y+ = 1{\cdot}0$ is generated for the ANSYS fluent using the Pointwise software[38].

As seen from Fig. 9(a), the ANSYS fluent with $k-\varepsilon$ realisable turbulence model shows the best accuracy of lift prediction at the cruise and stall regions. Figure 9(b) shows that Xfoil predicts aerofoil drag very close to the experimental value. The Spalart-Allmaras turbulence model and javafoil panel method tool also show the same trend; however, they are less accurate than $k-\varepsilon$ and Xfoil. The high drag of the Ansys fluent model is due to the viscous drag of the turbulent boundary layer, which is higher than that of the laminar. Xfoil uses a semi-empirical boundary layer and transition equation that shows better accuracy at low Mach numbers, where both laminar and turbulent flows exist.

According to the results shown in this section, it was decided to use the hybrid aerodynamic solver ANSYS fluent for the calculation of the lift and moment and Xfoil for the drag. A single

https://doi.org/10.1017/S0001924000011234 Published online by Cambridge University Press

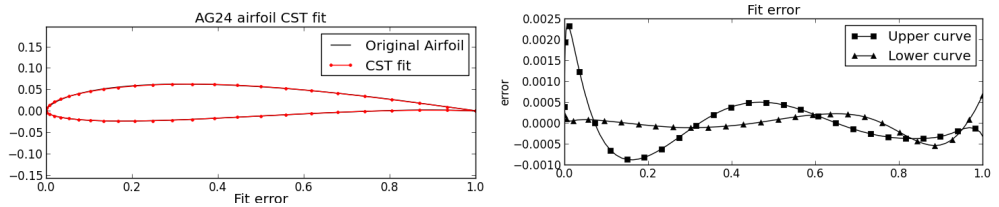
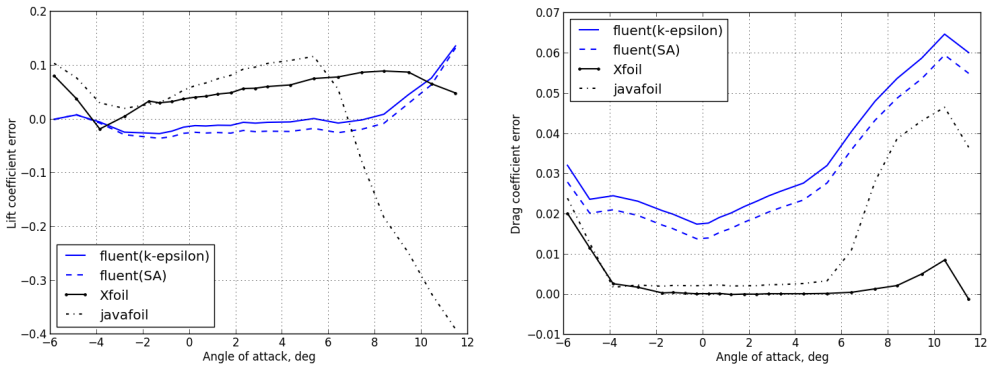


Figure 8 AG24 aerofoil representation using CST.



(a) Error of the lift coefficient vs. angle-of-attack (b) Error of the drag coefficient vs. angle-of-attack

Figure 9. Comparison of accuracy of different aerodynamic solvers.

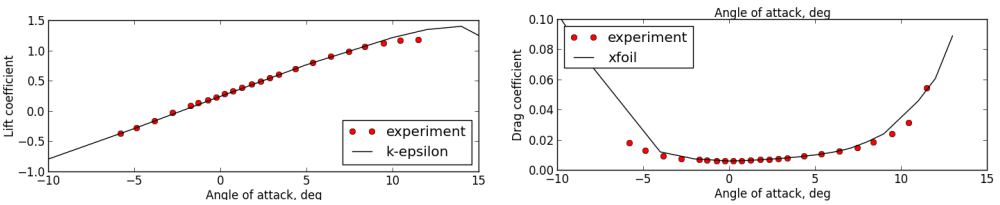


Figure 10. AG24 aerofoil aerodynamic analysis results comparison using the hybrid solver.

run of ANSYS fluent takes from one to three minutes for a single angle-of-attack on a desktop PC. A single run of Xfoil takes a couple of seconds.

The results of the aerodynamic analysis using the hybrid solver are shown in Fig. 10 for a baseline AG24 aerofoil compared with the experimental data[37]. The lift and drag coefficients of the AG24 aerofoil show good agreement with the experimental data of the AG24 aerofoil when using the hybrid aero solver.

4.3 Long endurance UAV aerofoil design optimisation using RENN

a. Long endurance UAV aerofoil and RENN integration process

The long endurance UAV aerofoil design optimisation is integrated into the RENN method, as shown in Fig. 11. The CST parameterisation method is used for aerofoil modelling. The Latin Hypercube method[28] is selected for creating the set of appropriate experimental points for the hybrid aero solver. The structured mesh is automatically generated for the different aerofoil configurations. The hybrid optimiser is used to search for a tentative optimal aerofoil configuration. Then, it is

https://doi.org/10.1017/S0001924000011234 Published online by Cambridge University Press

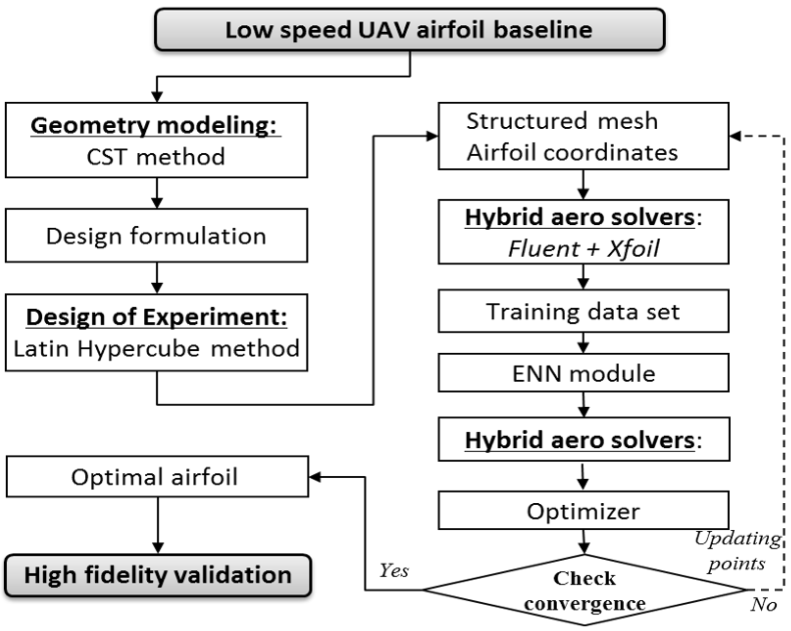


Figure 11. Long endurance UAV aerofoil design and RENN integration.

updated into the training data set if the tolerance is not satisfied. The optimal aerofoil is found and validated using the high fidelity analysis, as shown in Fig. 11.

b. UAV aerofoil design formulation

The minimisation of drag at cruise conditions is selected as an objective function for UAV aerofoil design. The low aerofoil drag at cruise conditions increases the range and endurance during cruise operation of the UAV. The constraints include the maximum lift coefficient, stall angle-of-attack, drag coefficient, and thickness ratio, as shown in the design formulation. The ten design variables representing the baseline UAV aerofoil AG24 with the lower and upper bounds are shown in Table 4. Subject to:

$$Minimise: f(x) = C_d \text{ at cruise condtion} \quad \ldots (13)$$

$$C_{lmax} \geq 1{\cdot}5$$
$$\alpha_{stall} \geq 14^\circ$$
$$C_d \leq C_{dbaseline} \text{ at } L/D_{max}$$
$$8\% \leq t/c \leq 14\%$$

The global sensitivity analysis is performed on ten geometry design variables using the Latin Hypercube method. A total of 100 experiments points are generated and executed by the hybrid aero solver. The scattered data of the ten design variables on the maximum lift coefficient, stall angle-of-attack, drag coefficient, and thickness ratio are shown in the Fig. 12. The results show that all 10 aerofoil geometry design variables are sensitive to the objective and constraints. Therefore, all 10 variables are considered into design optimisation loop.

https://doi.org/10.1017/S0001924000011234 Published online by Cambridge University Press

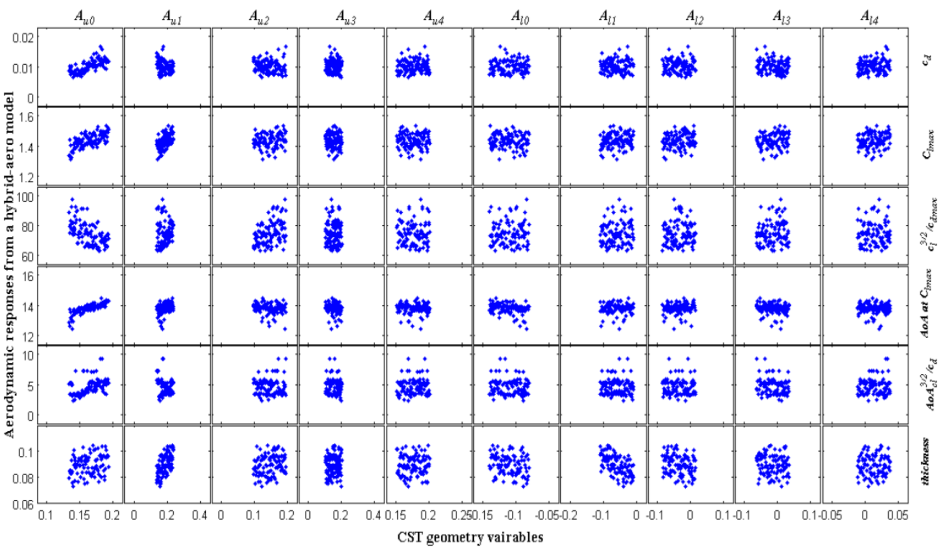


Figure 12. Aerofoil design variables sensitivity analysis to aerodynamic responses.

4.4 Optimal long endurance UAV aerofoil configuration

The optimal UAV aerofoil is presented in Table 5. The optimal aerofoil drag shows a 10·8% reduction compared with the baseline aerofoil AG24. The maximum lift coefficient and stall angle-of-attack constraints are active, as shown in Table 5. The optimal configuration using high fidelity analysis only and the RENN method are shown in Fig. 13 to compare with the baseline AG24. The optimal aerofoil configuration using the RENN method converges closely to the optimal aerofoil using the high fidelity analysis.

Table 4
Long endurance UAV aerofoil design variables by the cst geometry representation method

Design Variables	Baseline (AG24)	Lower bound	Upper bound
A_{u0}	0·1439	0·1339	0·1939
A_{u1}	0·1878	0·1378	0·2378
A_{u2}	0·1463	0·0963	0·1963
A_{u3}	0·1535	0·1035	0·2035
A_{u4}	0·1511	0·1511	0·2011
A_{l0}	–0·0901	–0·1401	–0·0801
A_{l1}	–0·0586	–0·1086	–0·0086
A_{l2}	–0·0349	–0·0849	0·0151
A_{l3}	–0·0143	–0·0643	0·0357
A_{l4}	0·0383	–0·0117	0·0383

https://doi.org/10.1017/S0001924000011234 Published online by Cambridge University Press

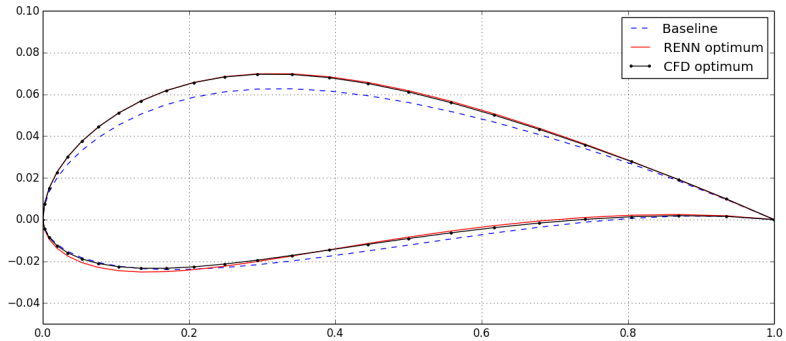


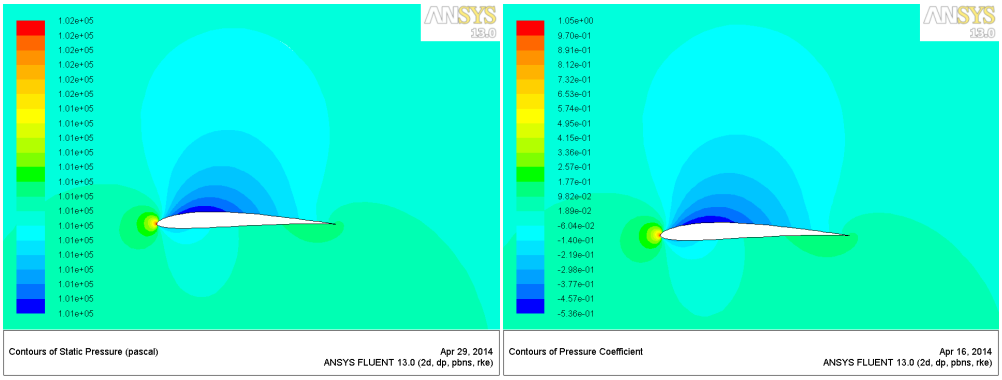
Figure 13. Baseline and optimum aerofoil shapes.

Table 5
Optimal long endurance UAV aerofoil configuration comparison

		Baseline (AG24)	Optimal high-lift low speed UAV aerofoil		
			High fidelity only	RENN	Units
Objective	Cd	0·0074	0·0066	0·0066	
Variables	A_{u0}	0·1439	0·1639	0·1639	
	A_{u0}	0·1878	0·2077	0·2078	
	A_{u0}	0·1463	0·1663	0·1663	
	A_{u0}	0·1535	0·1545	0·1629	
	A_{u0}	0·1511	0·1572	0·1511	
	A_{l0}	–0·0901	–0·0951	–0·1049	
	A_{l1}	–0·0586	–0·0529	–0·0548	
	A_{l2}	–0·0349	–0·0194	–0·0149	
	A_{l3}	–0·0143	–0·0052	–0·0009	
	A_{l4}	0·0383	0·0339	0·0383	
Constraints	C_{lmax}	1·4235	1·486	1·495	
	AoA at C_{lmax}	13·5459	13·89	13·99	deg·
	C_d at L/D_{max}	0·0074	0·0066	0·0066	
	t/c	8·44	8·97	9·08	%
f_{high} evaluations			423	88	
Computational time			35·1	6·6	hours

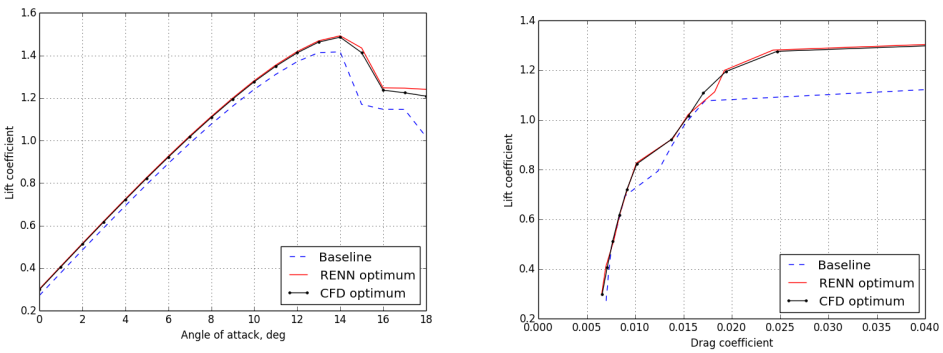
The pressure distribution of the optimal aerofoil for both the high fidelity and the RENN method shows similar behavior in Fig. 14. The optimal aerofoil lift and drag coefficient curves are presented in Fig. 15 and are compared with the baseline aerofoil AG24. Small differences in the stall angle-of-attack, maximum lift coefficient and thickness ratio, as shown in Table 5 and Fig. 15. The maximum difference occurs at a thickness ratio with 1·24% error compared with the high fidelity optimal configuration. On the contrary, the computational time saved is 81·2% in the RENN method compared with the full high fidelity analysis, as shown in Table 5. The significant improvement in computational time is obtained with very accurate results at the maximum error of 1·2 percent.

https://doi.org/10.1017/S0001924000011234 Published online by Cambridge University Press



(a) Optimal aerofoil using high-fidelity analysis only (b) Optimal aerofoil using the RENN method

Figure 14. Optimal aerofoil pressure distribution.



(a) Lift coefficient vs angle-of-attack (b) Drag vs lift coefficient

Figure 15. Baseline and optimum aerofoil polar comparison.

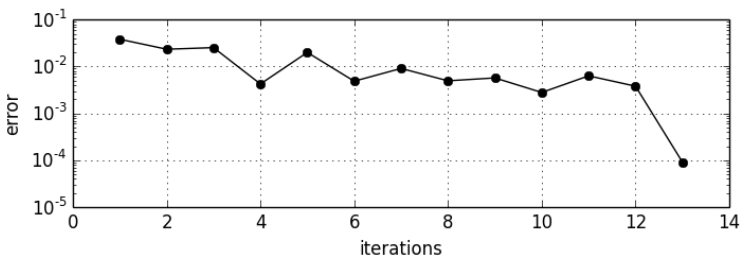


Figure 16. Design variable convergence history using the RENN method.

The RENN algorithm converges to a feasible optimum solution in 13 iterations. The total number of high fidelity function evaluations is then 88 (75 for surrogate initialisation and 13 evaluated during iterations). High fidelity optimisation has terminated with 423 high-fidelity function evaluations. Total computational time of the high fidelity analysis is 11·5hrs for RENN versus 56hrs for pure high-fidelity optimisation. Computational time of the Xfoil is negligible comparing to Ansys Fluent. The convergence history of the design variable is shown in Fig. 16. Here the error is the Euclidean distance between the optimum point at present and the previous iterations. The

https://doi.org/10.1017/S0001924000011234 Published online by Cambridge University Press

convergence rate is constant without large oscillations, which means it is a good approximation of the optimum point neighborhood.

$$error = \| x_n^* - x_{n-1}^* \| \quad \ldots (14)$$

The convergence of the objective and constraint functions is shown in Fig. 17. The approximated and exact function values almost exactly match the constraint functions after several iterations that refine the Neural Network in the optimum solution neighbourhood. Both constraint functions (c_{lmax}, α_{stall}) converged on the boundary within the constraint tolerance $\varepsilon_g = 10^{-3}$. Two identical medium sized UAVs with c_{lmax} difference of 10^{-3} will have stall speed difference order of 0·01ms^{-1} that is not significant. Stall angle-of-attack difference of 10^{-3} is also very small to affect overall aircraft performance. Thus $\varepsilon_g = 10^{-3}$ is small enough for given set of constraints. Tyan *et al*[39]. has succeeded for subsonic and transonic aerofoil design optimisation with 10^{-3} convergence tolerance and similar geometry parameterisation scheme.

5.0 CONCLUSION

The RENN method was developed and presented successfully. Its accuracy and feasibility were demonstrated with the help of a 2D numerical example and through the design of a two-member frame, which gave very accurate results when compared with the exact solution and the RSM. Thus, it is a promising approach for solving complex engineering design problems, nonlinear behavior and implicit functions with low turnaround time.

The RENN method was successfully applied for long endurance UAV aerofoil design optimisation in support of the CST geometry parameterisation method and high-fidelity analysis solver with ten design variables. The optimal UAV aerofoil improves the drag reduction by 10·8% and increases the maximum lift coefficient and stall angle-of-attack for both the RENN method and the high-fidelity analysis model. The convergence of the RENN method is reached at 13 iterations,

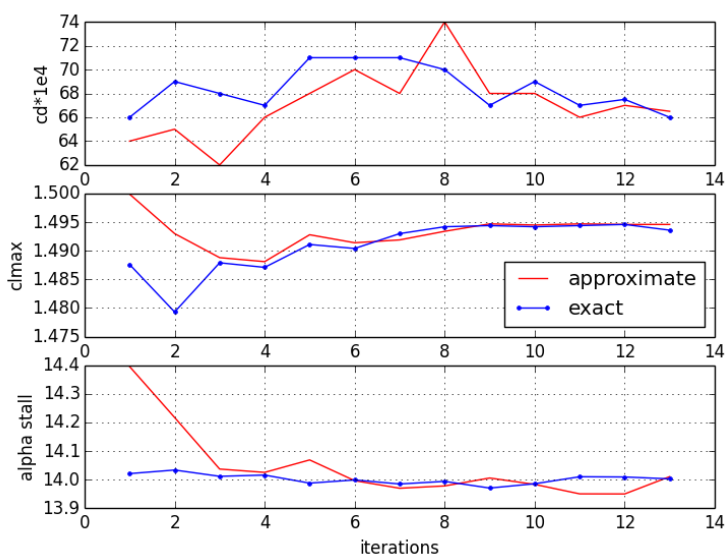


Figure 17. Objective and constraint functions convergence using the RENN method.

https://doi.org/10.1017/S0001924000011234 Published online by Cambridge University Press

totaling 88 high-fidelity evaluations in 6·6hrs, which saves 81·2% computational time when compared with the high-fidelity analysis while maintaining the maximum error at 1·2% compared with the optimal aerofoil results using high-fidelity analysis.

ACKNOWLEDGEMENT

This work was supported by the National Research Foundation of Korea (NRF) [grant NRF-2014R1A2A2A01003833] funded by the Korean government (MSIP) and 2014 KU Brain Pool, Konkuk University, Republic of Korea. The corresponding author email: jwlee@konkuk.ac.kr.

REFERENCES

1. CHANGYU, S., LIXIA, W. and QUAN, L. Optimization of injection molding process parameters using combination of artificial neural network and genetic algorithm, *Sci Direct J*, 2007, **183**, (2-3), pp 412–418.
2. OZCELIK, B. and ERZURUMLU, T. Comparison of the warpage optimization in the plastic injection molding using ANOVA, neural network model and genetic algorithm, *J Materials Processing Technology*, 2006, **171**, pp 437–445.
3. MOK, S.L., KWONG, C.K. and LAU, W.S. A hybrid neural network and genetic algorithm approach to the determination of initial process parameters for injection molding, *Int J Advanced Manufacturing Tech*, September 2001, **18**, pp 404-409.
4. PARK, K.H., JUN, S.O. and BAEK, S.M. *et al*, Reduced-order model with an artificial neural network for aerostructural design optimization, *J Aircr*, July-August 2013, **50**, (4).
5. MAZHAR, F., KHAN, A.M., CHAUDHRY, I.A. and AHSAN, M. On using neural networks in UAV structural design for CFD data fitting and classification, *Aerospace Science and Technology*, 2013, **30**, pp 210–225.
6. ATHAR KHARAL, A. and SALEEM, A. Neural networks based aerofoil generation for a given C_p using Bezier–PARSEC parameterization, *Aerospace Science and Technology*, 2012, **23**, pp 330–344.
7. SAMY, I., POSTLETHWAITE, I. and GU, D.-W. Neural-network-based flush air data sensing system demonstrated on a mini air vehicle, *J Aircr*, January-February 2010, **47**, (1).
8. RAI, M.M. and MADAVAN, N.K. Aerodynamic design using neural networks, *AIAA J*, 2000, **38**, (1), pp 173-182.
9. SAIJA L, K.K., GANGULI, R. and VISWAMURTHY, S.R. Optimization of helicopter rotor using polynomial and neural network metamodels, *J Aircr*, March-April 2011, **48**, (2).
10. PATNAIK, S.N., CORONEOS, R.M., GUPTILL, J.D. and HOPKINS, D.A. Subsonic aircraft design optimization with neural network and regression approximators, *J Aircr*, September-October 2005, **42**, (5).
11. SHYY, W., PAPILA, N., VAIDYANAT HAN, R. and TUCKER, K. Global design optimization for aerodynamics and rocket propulsion components, *Progress in Aerospace Sciences*, 2001, **37**, pp 59-118.
12. OROUMIEH, M.A.A., MALAEK, S.M.B., ASHRAFIZAA DEH, M. and TAHERI, S.M. Aircraft design cycle time reduction using artificial intelligence, *Aerospace Science and Technology*, 2013, **26**, pp 244–258.
13. SINHA, M., AYILLIAT, R., AJOY, K.,GHOSH, K. and MISRA, A. High angle-of-attack parameter estimation of cascaded fins using neural network, *J Aircr,* January-February 2013, **50**.
14. HORN, J.F., SCHMIDT, E.M., BRIAN, R., GEIGER, B.R. and DEANGELO, M.P. Neural network-based trajectory optimization for unmanned aerial vehicles, *J Guidance, Control, and Dynamics*, March-April 2012, **35**, (2).
15. HACIOGLU, A. Fast evolutionary algorithm for aerofoil design via neural network, *AIAA J*, September 2007, **45**, (9).
16. QUEIPO, N.V., HAFTKA, R.T., SHYY, W., GOEL, T., VAIDYNAT HAN, R. and TUCKER, P.K. Surrogate based analysis and optimization, *Progress in Aerospace Sciences,* January 2005, **41**, (1), pp 1-28.
17. FORRESTER, A.I.J. and KEANE, A.J. Recent advances in surrogate-based optimization, *Progress in Aerospace Sciences*, January-April 2009, **45**, 1-3, pp 50-79.
18. KOZIEL, S., ECHEVERRÍA-CIAURRI, D. and LEIFSSON, L. Surrogate-based methods, in KOZIEL S. and YANG, X.S. (Eds) *Computational Optimization, Methods and Algorithms, Series: Studies in Computational Intelligence*, Springer-Verlag, pp 33-60, 2011.
19. KOZIEL, S. and LEIFSSON, L. Multi-Level Surrogate-Based Aerofoil Shape Optimization, 51st AIAA Aerospace Sciences Meeting including the New Horizons Forum and Aerospace Exposition, Grapevine, Texas, USA, 7-10 January, 2013.

https://doi.org/10.1017/S0001924000011234 Published online by Cambridge University Press

20. KOZIEL, S. and LEIFSSON, L. Surrogate-based aerodynamic shape optimization by variable-resolution models, *AIAA J*, 2013, **51**, (1), pp 94-106.
21. KOZIEL, S. and LEIFSSON, L. Knowledge-Based Aerofoil Shape Optimization Using Space Mapping, 30th AIAA Applied Aerodynamics Conference, New Orleans, Louisiana, USA, 25-28 June 2012.
22. S. I. Inc., JMP(R) User Guide. 2nd Edition, Cary, NC: SAS Institute Inc, 2009.
23. MYERS, R.H. and MONTGOMERY, D.C. *Response Surface Methodology: Process and Product Optimization Using Designed Experiments*, Wiley-Interscience, 1995.
24. HAGAN, M.T., DEMUTH, H.B. and BEALE, M.H. *Neural Network Design*, PWS, 1996.
25. NGUYEN, D. and WIDROW, B. Improving the learning speed of 2-layer neural networks by choosing initial values of the adaptive weights, Int Joint Conf Neural Networks, June 1990, **3**, pp 21–26.
26. MACKAY, D.J.C. A practical Bayesian process for backprop networks, *Neural Computation J*, 1992, **4**, pp 448–472.
27. MATLAB 2013, Neural Networks Toolbox, http://www.mathworks.co.kr/
28. GOLDBERG, D.E. *Genetic Algorithms in Search, Optimization, and Machine Learning*, Addison-Webley-Professional, 1989.
29. ARORA, J.S. *Introduction to Optimum Design*, 2nd ed, Elsevier Academic Press, 2004.
30. JEON, K.-S., LEE, J-W. and BYUN, Y.-H. Repetitive Response Surface Enhancement Techniques through Design Space Transformation and Sub-Optimization ICAS 25th Int Congress of the Aeronautical Sci, Hamburg, Germany, September 2006.
31. KULFAN, B.M. A universal parametric geometry representation method CST, *J Aircr*, January–February 2008, **45**, (1).
32. VU, N.A., LEE, J-W. and SHU, J. Aerodynamic design optimization of helicopter rotor blades including aerofoil shape for hover performance, *Chinese J Aeronautics*, 2013, **26**, (1), pp 1-8.
33. AZAMATOV, A., LEE, J-W. and BYUN, Y.-H. Comprehensive aircraft configuration design tool for integrated product and process development, Advances in Engineering Software, 2011, **42**, pp 35-49.
34. ANSYS FLUENT flow modelling and simulation software, Ansys Inc.
35. DRELA, M. Xfoil program, available: http://web.mit.edu/drela/Public/web/xfoil/
36. JavaFoil – Analysis of Aerofoils, http://www.mh-aerotools.de/aerofoils/javafoil.htm
37. WILLIAMSON, A.G., MCGRANAHAN, B.D., BROUGHTON, B.A., DETERS, R.W., BRANDT, J.B. and SELIG, M.S. Summary of low-speed aerofoil data, Department of Aerospace Engineering, University of Illinois at Urbana-Champaign, Illinois, USA, 2012.
38. Gridgen – Pointwise, http://www.pointwise.com/gridgen/
39. TYAN, M., VAN NGUYEN, N. and LEE, J.-W. Improving variable fidelity modelling by exploring global design space and radial basis functions networks for aerofoil design, *Engineering Optimization Journal*, Taylor & Francis, DOI: 10.1080/0305215X.2014.941290, 2014.

https://doi.org/10.1017/S0001924000011234 Published online by Cambridge University Press